

How many spin liquids are there in $\text{Ca}_{10}\text{Cr}_7\text{O}_{28}$?

Rico Pohle,^{1,*} Han Yan,^{1,†} and Nic Shannon^{1,‡}

¹Okinawa Institute of Science and Technology Graduate University, Onna-son, Okinawa 904-0412, Japan

(Dated: November 13, 2017)

The search for novel phases of matter is a central theme of modern physics, with some of the most intriguing examples provided by the spin liquids found in magnets with competing, or “frustrated” interactions. $\text{Ca}_{10}\text{Cr}_7\text{O}_{28}$, a novel spin-1/2 magnet with a bilayer breathing-kagome lattice, has properties which differ from any known spin liquid. However, understanding $\text{Ca}_{10}\text{Cr}_7\text{O}_{28}$ presents a significant challenge, because of its complex frustration. Here we use large-scale molecular-dynamics simulation to explore the origin of spin-liquid behaviour in $\text{Ca}_{10}\text{Cr}_7\text{O}_{28}$. We uncover qualitatively different behaviour on different timescales, and argue that ground state of $\text{Ca}_{10}\text{Cr}_7\text{O}_{28}$ is born out of a slowly-fluctuating “spiral spin liquid”, while faster fluctuations echo the U(1) spin liquid found in the kagome antiferromagnet. These results provide a concrete scenario for spin-liquid behaviour in $\text{Ca}_{10}\text{Cr}_7\text{O}_{28}$, and highlight the possibility of spin liquids existing on multiple timescales.

The search for novel quantum phases and excitations is one of the defining themes of modern physics, reaching from the large-scale structure of the universe, to many-body physics on the scale of few Angstrom. Quantum spin systems, and in particular, magnets with competing or “frustrated” interactions, occupy a special place in this endeavour, and have consistently proved to be one of the most fruitful places to look for new phases of matter. While conventional magnets order at low temperatures, and exhibit excitations with the character of spin waves, frustrated magnets display a far richer behaviour. In particular, they can support a *quantum spin liquid* (QSL), a massively-entangled phase of matter in which evades all conventional forms of magnetic order, and instead supports entirely new forms of excitation, often with topological character [1]. The discussion of quantum spin liquids has a long history [2], but until recently experimental realisations remained scarce [3]. Happily, however, the past few years have seen an explosion in the number systems under study, with examples including quasi-2D organics [3, 4], thin films of ^3He [5], spin-1/2 magnets with a Kagome lattice [6], “Kitaev” magnets with strongly anisotropic exchange [7–10], and quantum analogues of spin ice [11–14].

An exciting new arrival on this scene is the quasi-2D magnet $\text{Ca}_{10}\text{Cr}_7\text{O}_{28}$, a system which appears to have qualitatively different properties from any previously-studied spin liquid. First studied for its unusual chemistry [15, 16], recent experiments identified $\text{Ca}_{10}\text{Cr}_7\text{O}_{28}$ as a system where spin-1/2 Cr^{5+} ions occupy sites of a bilayer breathing Kagome (BBK) lattice with extremely complex frustration [17–19]. Heat-capacity, neutron-scattering and μSR experiments on $\text{Ca}_{10}\text{Cr}_7\text{O}_{28}$, find no traces of magnetic order down to a temperature of 19 mK, two orders of magnitude lower than the scale of interactions [17]. Meanwhile, inelastic neutron scattering [17, 18] reveals “bow-tie” like structure at intermediate to high energies [Fig. 1a,1c], and qualitatively different scattering, more reminiscent of a ring, at lower energies [Fig. 1e]. Parallel pseudo-fermion functional renormalisation group calculations suggest that the ground state of $\text{Ca}_{10}\text{Cr}_7\text{O}_{28}$ should be a quantum spin liquid, characterised by a “ring” in the static structure factor $S(\mathbf{q}, \omega = 0)$ [17].

None the less, the origin of this spin liquid, and the attendant ring in scattering, remain obscure [17–19].

In this Article we address the nature and origin of spin liquid behaviour in $\text{Ca}_{10}\text{Cr}_7\text{O}_{28}$, starting from the microscopic model introduced by Balz *et al.* [17–19], and using large-scale molecular dynamics simulation to explore its semi-classical spin dynamics. We find that the spins continue to fluctuate down to very low temperatures, and that fluctuations on different timescales encode signatures usually associated with two distinct types of spin liquid; a slowly-fluctuating “spiral spin liquid” characterised by a degenerate “ring” of spin configurations; and, on shorter timescales, “bow-tie” structure reminiscent of the pinch points observed in the Kagome-lattice antiferromagnet. Applying a magnetic field opens a gap to transverse spin excitations; we argue that the quantum spin-liquid ground state in $\text{Ca}_{10}\text{Cr}_7\text{O}_{28}$ is born out of the slow fluctuations associated with the degenerate “ring” at a field of 1 T, where this gap closes. We also offer a simple explanation of this degenerate ring, through a mapping on to an effective spin-3/2 Heisenberg model on a honeycomb lattice. These results provide a concrete scenario for spin-liquid behaviour in $\text{Ca}_{10}\text{Cr}_7\text{O}_{28}$, and highlight the possibility of different spin liquids supporting qualitatively different properties on different timescales.

The first surprise in $\text{Ca}_{10}\text{Cr}_7\text{O}_{28}$ is a chemical one; the highly-unusual, spin-1/2, Cr^{5+} valence state [15]. Structurally, $\text{Ca}_{10}\text{Cr}_7\text{O}_{28}$ has much in common with the quantum dimer system SrCr_2O_8 [20, 21]. However the inclusion of non-magnetic Cr^{6+} ions converts the triangular lattice of SrCr_2O_8 into a bilayers of a “breathing” Kagome lattice [19] — cf. Fig. 2a. These bilayers have a six-site unit cell, and very low symmetry (R3c) [16, 19].

The magnetic properties of $\text{Ca}_{10}\text{Cr}_7\text{O}_{28}$ are every bit as exotic as its chemistry. Curie-law fits to magnetic susceptibility suggest predominantly ferromagnetic (FM) exchange interactions, with $\theta_{\text{CW}} = 2.35$ K [18]. Meanwhile, the lack of magnetic anisotropy, coupled with the fact that $\text{Ca}_{10}\text{Cr}_7\text{O}_{28}$ is a good insulator, suggest that a Heisenberg model should provide a good starting point for understanding its magnetism [17–19]. At that point, however, all semblance of conven-

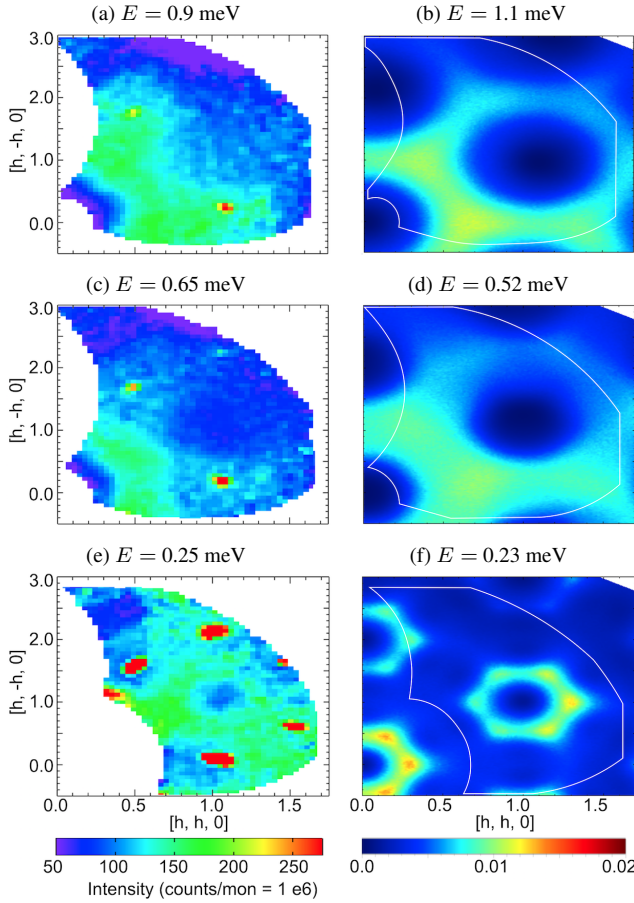


Figure 1. **Fluctuations in the spin-liquid phase of $\text{Ca}_{10}\text{Cr}_7\text{O}_{28}$, showing \mathbf{q} -dependent structure on different timescales.** (a) Cut through inelastic neutron scattering (INS) data for $\text{Ca}_{10}\text{Cr}_7\text{O}_{28}$ at high energy, showing “bow-tie” structure centered on $(0.5, 0.5, 0)$. (b) Equivalent results from molecular dynamics (MD) simulations of \mathcal{H}_{BBK} [Eq. (1)]. (c) INS data for $\text{Ca}_{10}\text{Cr}_7\text{O}_{28}$ at intermediate energy, also showing “bow-tie” structure. (d) Equivalent results from MD simulation. (e) INS data for $\text{Ca}_{10}\text{Cr}_7\text{O}_{28}$, suggesting a “ring” of scattering at low energy. (f) Equivalent results from MD simulation. Experimental data is reproduced from [17]; details of simulations are given in the text. INS experiments were carried out at $T = 90$ mK; MD simulations at $T = 222$ mK.

tional magnetism ceases. $\text{Ca}_{10}\text{Cr}_7\text{O}_{28}$ does not order down to the lowest temperatures measured, with persistent spin dynamics found in μSR down to 19 mK [17]. Consistent with this, neutron scattering experiments find no magnetic Bragg peaks down to 90 mK [17, 18]. Instead, scattering is predominantly inelastic and highly-structured, with results at 0.25 meV showing hints of a ring suggested at $(1, 1, 0)$ [Fig. 1e], while scattering at 0.90 meV suggests a bow-tie like structure centered on $(0.5, 0.5, 0)$ [Fig. 1a].

Table I. **Exchange interactions in bilayer breathing-Kagome model of $\text{Ca}_{10}\text{Cr}_7\text{O}_{28}$, and mapping onto effective honeycomb-lattice model.** Magnetic interactions within the spin-1/2 bilayer breathing-Kagome (BBK) model, \mathcal{H}_{BBK} [Eq. (1)], are labelled following the convention of Balz *et al.* [17, 18], as illustrated in Fig. 2a. Experimental values are taken from fits to inelastic neutron scattering in applied magnetic field [17, 18]. The mapping onto an effective spin-3/2 honeycomb-lattice (HCM) model, \mathcal{H}_{HCM} [Eq. (2)], is illustrated in Fig. 2a.

\mathcal{H}_{BBK} [Eq. (1)]	$\text{Ca}_{10}\text{Cr}_7\text{O}_{28}$ [17, 18]	\mathcal{H}_{HCM} [Eq. (2)]
J_0	$-0.08(4)$ meV	J_1
J_{21}	$-0.76(5)$ meV	–
J_{22}	$-0.27(3)$ meV	–
J_{31}	$0.09(2)$ meV	J_2
J_{32}	$0.11(3)$ meV	J_2

In contrast with SrCr_2O_8 [20, 21], the magnetization of $\text{Ca}_{10}\text{Cr}_7\text{O}_{28}$ rises rapidly in applied magnetic field, implying a gapless ground state [18]. The magnetisation also saturates at the relatively low field of 13 T, making it possible to carry out inelastic neutron scattering (INS) experiments in the field-polarised state [17, 18]. These reveal gapped, two-dimensional spin-wave excitations [Fig. 4a], well-described by a Heisenberg model for single bilayer [17, 18]

$$\mathcal{H}_{\text{BBK}} = \sum_{\langle ij \rangle} J_{ij} \mathbf{S}_i \cdot \mathbf{S}_j - \mathbf{B} \cdot \sum_i \mathbf{S}_i, \quad (1)$$

where \mathbf{B} is the external magnetic field, and J_{ij} the exchange interaction on the first-neighbour bond ij [cf. Table I]. The strongest exchange interactions are FM, and occur within triangular plaquettes in alternating layers [Fig. 2a]. On reducing magnetic field, the sharp features associated with spin-waves retain their identity, but move down in energy, with the lowest-lying band vanishing into the elastic line below about 1 T [18]. At the same time, heat capacity measurements show a systematic change at 1 T, consistent with the closing of a gap [18].

While spin-liquid behaviour has been discussed in a wide range of two-dimensional systems [1–10], the origin of the gapless spin liquid in $\text{Ca}_{10}\text{Cr}_7\text{O}_{28}$ presents an entirely new challenge to theory. In addition to experiment, Balz *et al.* [17] present the results of a pseudo-fermion functional renormalisation group (PFFRG) analysis of \mathcal{H}_{BBK} [Eq. (1)]. These calculations provide information about the ground-state properties of the model, including its static structure factor, $S(\mathbf{q}, \omega = 0)$. Tantalizingly, for parameters taken from experiment, PFFRG calculations are consistent with a spin-liquid ground state, and predict a ring of scattering in $S(\mathbf{q}, \omega = 0)$, centered on $(1, 1, 0)$ [17]. However, because of the involved nature of the calculations, and complexity of the model, the origin of this ring structure remains obscure. And, for the time being at least, a direct comparison with INS results above the elastic line is out of reach. The challenge, then, is to explain how the seemingly-simple magnetism of

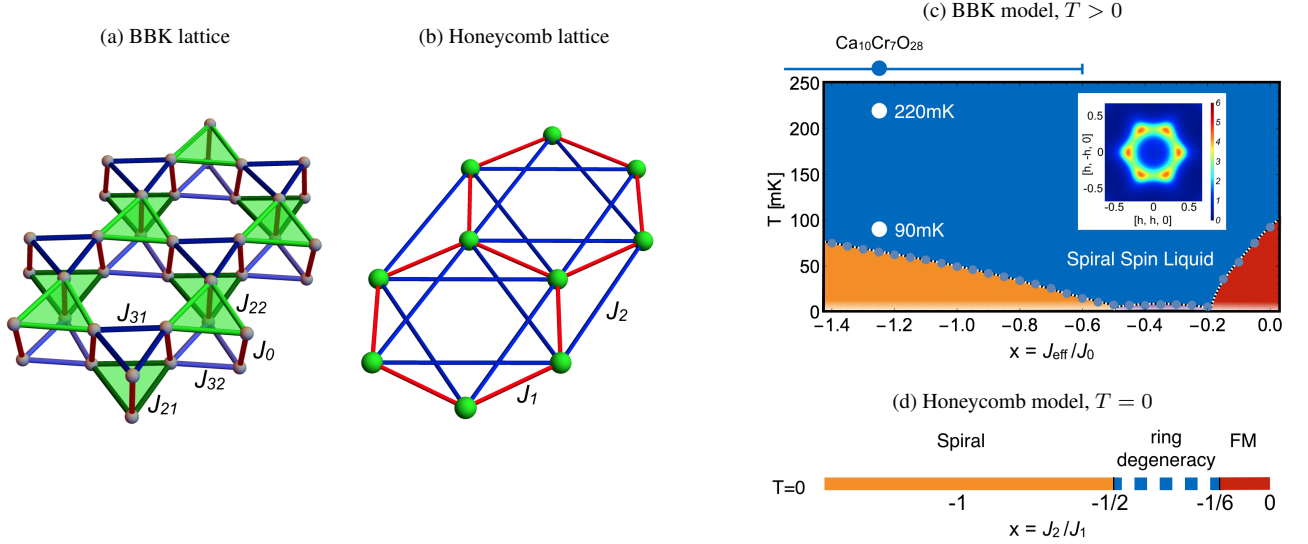


Figure 2. **Magnetic interactions in $\text{Ca}_{10}\text{Cr}_7\text{O}_{28}$ and mapping onto effective Honeycomb-lattice model.** (a) Bilayer breathing Kagome (BBK) lattice of spin-1/2 Cr^{5+} ions in $\text{Ca}_{10}\text{Cr}_7\text{O}_{28}$. Interactions are labelled following the conventions of Balz *et al.* [17, 18] (cf. Table I). (b) Effective honeycomb lattice formed by spin-3/2 moments on FM plaquettes. (c) Finite-temperature phase diagram of the BBK model, Eq. (1), as determined by classical Monte Carlo simulation, allowing $J_{\text{eff}} \equiv J_{31} = J_{32}$ to vary, with all other parameters taken from $\text{Ca}_{10}\text{Cr}_7\text{O}_{28}$. Dotted lines correspond to peaks in the specific heat $C(T)$, and indicate the onset of correlations corresponding to spiral/ferromagnetic states at low temperature. White spots show parameter-ratio and temperatures associated with inelastic neutron-scattering experiments on $\text{Ca}_{10}\text{Cr}_7\text{O}_{28}$ [17, 18]. **Inset:** “ring” in equal-time structure factor $S(\mathbf{q})$, characteristic of the spiral spin liquid. (d) Classical ground state of the effective honeycomb-lattice model, Eq. (2), following [22, 23]. The spiral spin liquid can be traced to a highly-degenerate manifold of classical ground states occurring for $-1/2 < x < -1/6$.

$\text{Ca}_{10}\text{Cr}_7\text{O}_{28}$ in high magnetic field, evolves into an entirely new form of gapless spin liquid for fields of less than 1 T.

RESULTS

To address the origin of spin liquid behaviour in $\text{Ca}_{10}\text{Cr}_7\text{O}_{28}$ we have used semi-classical molecular dynamics (MD) simulation of \mathcal{H}_{BBK} [Eq. (1)] to explore how spin excitations evolve as function of magnetic field. Within this approach, spin configurations are drawn from a classical Monte Carlo simulation of \mathcal{H}_{BBK} , carried out at finite temperature, and evolved according to the Heisenberg Equations of Motion [24–26]. We concentrate on a single bilayer, with parameters taken from experiment [cf. Table I].

The results of such a simulation, carried out for a temperature of $T = 222$ mK, in the absence of magnetic field ($B = 0$ T), are documented in the first Animation given in the Supplementary Information [27]. As the Animation shows, the spins continue to fluctuate, even at this low temperature, and parallel calculations of the equal-time structure factor $S(\mathbf{q})$ reveal a “a ring” structure, with no signs of long range order [cf. Inset to Fig. 2c]. On closer inspection, the simulation reveals that the spins exhibit both slow and fast dynamics, and that these have very different character, with a slow precession of locally collinear spins, mixing with fast fluctuations of seemingly-uncorrelated spins. (For clarity, in the Animation, spins which rotate quickly have been coloured

red).

All of these facts are consistent with the observation that $\text{Ca}_{10}\text{Cr}_7\text{O}_{28}$ enters a spin-liquid state at low temperatures, in which the fluctuations on different timescales show qualitatively different character. And the results of the MD simulations also stand up to a more quantitative comparison with experimental data. In Fig. 1, we show simulation results for the dynamical structure factor $S(\mathbf{q}, \omega)$, side-by-side with results from INS taken from [17]. To facilitate comparison, simulation results have been convoluted with a Gaussian mimicking experimental resolution, and a magnetic form factor appropriate to a Cr^{5+} ion. Both experiment and theory show broad “bow-tie” like structures at intermediate to high energy, and rings of scattering at low energy. (Bright “spots” seen in INS near to zone centers represent scattering from phonons, and do not form part of the magnetic signal [17]).

Clearly, the MD simulations capture important elements of the physics of $\text{Ca}_{10}\text{Cr}_7\text{O}_{28}$. Moreover, the “ring” found at low energies in MD simulation corresponds exactly to the ring found in the static structure factor $S(\mathbf{q}, \omega = 0)$ in PFFRG calculations [17] — cf. Fig. 3. The question which remains, is what does this tell us about the nature and origin of the spin-liquid state?

To gain more insight into this question, we have used MD simulation to track the evolution of spin dynamics from the saturated state at high magnetic field, into the spin liquid at $B = 0$ T. In Fig. 4 we show a comparison of INS results and MD simulation for a magnetic field of $B = 11$ T. Param-

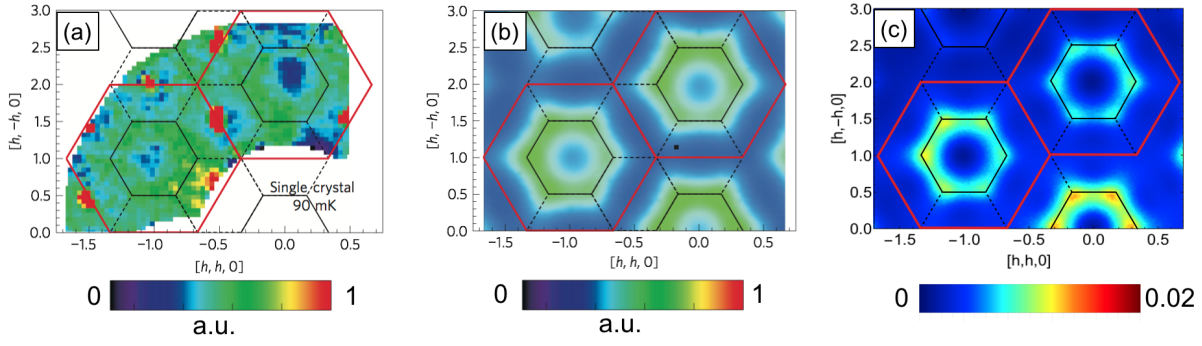


Figure 3. **Comparison of “ring” structure in spin correlations, as revealed by experiment and simulation.** (a) Dynamical structure factor measured in inelastic neutron scattering (INS) experiments on $\text{Ca}_{10}\text{Cr}_7\text{O}_{28}$ at $T = 90$ mK, $E = 0.25$ meV, reproduced from [17]. (b) Pseudo-Fermion Functional Renormalisation Group (PFFRG) results for static structure factor $S(\mathbf{q}, \omega = 0)$, also reproduced from [17], showing a ring-structure near to the Brillouin Zone (BZ) boundary. (c) Equivalent Molecular Dynamics (MD) simulation results for $S(\mathbf{q}, \omega)$ at $T = 222$ mK, $\hbar\omega = 0.23$ meV, showing the same ring structure.

ters for the MD simulation have been taken from experiment [cf. Table I] and, following [18], results have been convoluted with a Gaussian of FWHM = 0.2 meV, mimicking finite experimental resolution. The agreement between simulation and experiment is excellent.

Both experiment and simulation show excitations on three different energy scales; each of these corresponds to two bands of nearly-degenerate, transverse, spin-wave excitations [18]. The excitations at higher and intermediate energy are similar, but those at lower energy have a very different character, and contribute in different ways to the equal-time structure factor $S(\mathbf{q})$. In Fig. 4c, we show the results for the dynamical structure factor $S(\mathbf{q}, \omega)$, integrated over a range of energies corresponding to the two highest-energy spin-wave modes. Equivalent results for the intermediate-energy excitations are shown in Fig. 4d. Both exhibit “bow-tie” structures — e.g. centred on $\mathbf{q} = (0.5, 0.5, 0)$ — which link to form a broad network of scattering within the $[h, l, 0]$ plane. Meanwhile, equivalent calculations for the low-energy spin excitations show that their spectral weight is concentrated within the “holes” in this network [Fig. 4e].

As magnetic field is reduced, the gap to each band of excitations reduces, as illustrated in Fig. 5. At the same time, the individual character of spin excitations at different energy scales becomes easier to resolve; “bow-tie” patterns become more clearly marked at higher energies [Fig. 5c and Fig. 5c], and low-energy fluctuations start to form a ring at the zone boundary [Fig. 5e]. For this value of field, a large part of the spectral weight in experiment is obscured by quasi-elastic scattering, and it is hard to estimate whether the gap to transverse spin excitations is open or closed [Fig. 5a]. However in simulation, it is clear that the gap remains open [Fig. 5b — see also Fig. S1d5 of Supplementary Information]. The gap to transverse excitations finally closes at $B = 1$ T, as shown in Fig. 6, marking the onset of the low-field spin liquid phase. The critical value of field obtained from simulation, $B = 1.0(5)$ T, is in good correspondence with thermodynamic measurements, which suggest the onset of gapless spin-liquid behaviour at

$B = 1$ T [17].

We are now in position to address a crucial question, so far as the nature of the spin liquid is concerned: what is the nature of the spin correlations at the point at which this gap closes? We address first the “ring” seen in the lowest-energy excitations in MD simulation, and in the PFFRG calculations at $\omega = 0$. Ring-degeneracies of this form are familiar from a range of models which display spin-liquid ground states [22, 23, 28, 29]. Classically, they can be understood as an ensemble of degenerate spirals, and have been dubbed “spiral spin liquids” [30]. In the present case, we can also easily understand the origin of the “ring” degeneracy. The strongest exchange interactions in $\text{Ca}_{10}\text{Cr}_7\text{O}_{28}$ are FM and occur on alternating plaquettes [cf. Fig. 2a]. At low energies, these FM plaquettes behave like a honeycomb lattice of effective spin-3/2 moments [cf. Fig. 2b]

$$\mathcal{H}_{\text{HCM}} = J_1 \sum_{\langle ij \rangle_1} \mathbf{S}_i \cdot \mathbf{S}_j + J_2 \sum_{\langle ij \rangle_2} \mathbf{S}_i \cdot \mathbf{S}_j, \quad (2)$$

with FM J_1 and AF J_2 [cf. Table I]. For $-1/2 \leq J_2/J_1 \leq -1/6$, the classical ground state of \mathcal{H}_{HCM} is known to be a degenerate set of spirals with wave vectors belonging to a ring [22], providing all of the ingredients needed to form a classical spin liquid [29]. And a quantum spin liquid, occurring for a somewhat broader range of parameters, is indicated in exact-diagonalisation studies of the corresponding spin-1/2 model [23].

Experimental estimates for $\text{Ca}_{10}\text{Cr}_7\text{O}_{28}$ yield $-3.1 \approx J_2/J_1 \approx -0.6$ [Table I], neighbouring the degenerate regime, but within a region of parameter space where the classical ground state of \mathcal{H}_{HCM} is an ordered spiral [Fig. 2d]. In keeping with this, our MC simulations show a strong anomaly in heat capacity at $T \approx 60$ mK, consistent with a tendency to order. However, above this temperature, the entropy associated with ring-degeneracy predominates, and classical MC simulations find a spiral-spin liquid, characterised by a ring in $S(\mathbf{q})$ [Fig. 2d]. And, given that line-degeneracies lead to logarithmic divergences

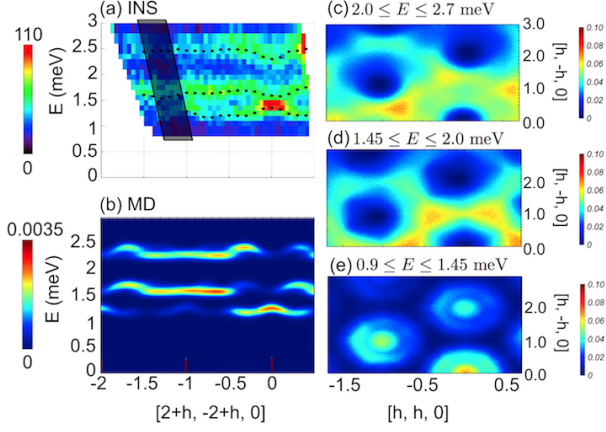


Figure 4. **Spin excitations of $\text{Ca}_{10}\text{Cr}_7\text{O}_{28}$ in high magnetic field ($B = 11$ T).** (a) Spin excitations measured in inelastic neutron scattering [17], integrated over $\Delta\mathbf{q} = \pm 0.1$ rlu perpendicular to the cut in reciprocal space, showing dispersing excitations with three distinct energy scales. The dashed line shows a fit to linear spin wave (LSW) theory, for parameters given in Table I. (b) Equivalent results for the dynamical structure factor $S(\mathbf{q}, \omega)$, taken from molecular dynamics (MD) simulations of \mathcal{H}_{BBK} [Eq. (1)], with parameters taken from experiment [Table I]. (c)–(e) Contribution to the energy-integrated structure factor $S(\mathbf{q})$ coming from excitations in the higher-, intermediate- and lower-energy bands visible in (b), within MD simulation. Bow-tie like features are clearly visible in the intermediate-energy bands, shown in (d).

in spin-wave corrections in two dimensions [31, 32], we anticipate that any classically-ordered ground state would quickly be eliminated by quantum fluctuations.

We now turn to the “bow-tie” features observed at finite energy. Structure of this form is already familiar from the Kagome-lattice antiferromagnet, where they have the interpretation of “pinch points”, singular points in scattering associated with a local constraint on spin configurations [26, 33, 34]. As such, they are a signal feature of an entirely different kind of spin liquid — a Coulombic phase with an emergent $U(1)$ gauge structure [35]. The pinch points seen in simulations of $\text{Ca}_{10}\text{Cr}_7\text{O}_{28}$ [cf. Fig. 4] are encoded in bands of transverse spin excitations. These bands occur in pairs and, at lower value of magnetic field, overlap with much broader bands of longitudinal excitations, documented in the Supplementary Information. It is possible to understand these pinch points through the dynamical stability of a local constraint, a theme which will be explored further elsewhere [36]. Meanwhile, the continuous evolution of the “bow-tie” structure from $B = 11$ T [Fig. 4c,d] to $B = 0$ T [Fig. 7c,d], suggests that this local constraint also has a role to play in the fluctuations of the spin liquid.

Armed with these new insights, we are finally in a position to return to simulations carried out in the absence of magnetic field, and interpret the very different structure seen at different timescales. In the Second Animation given in the Supplementary Information [37], we exhibit the same results as shown in

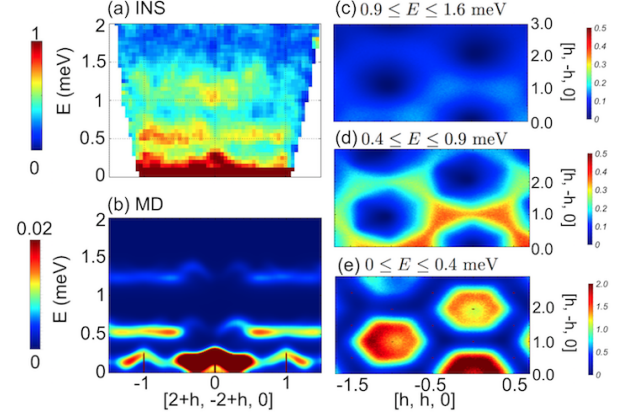


Figure 5. **Spin excitations of $\text{Ca}_{10}\text{Cr}_7\text{O}_{28}$ in intermediate magnetic field ($B = 2$ T).** (a) Spin excitations measured in inelastic neutron scattering [17], integrated over $\Delta\mathbf{q} = \pm 0.2$ rlu perpendicular to the cut in reciprocal space. (b) Equivalent results from molecular dynamics (MD) simulations of \mathcal{H}_{BBK} [Eq. (1)], with parameters taken from experiment [Table I]. (c)–(e) Contribution to the energy-integrated structure factor $S(\mathbf{q})$ coming from excitations in the higher-, intermediate- and lower-energy bands visible in (b), within MD simulation. Bow-tie like features are clearly visible in the intermediate-energy bands, shown in (d). Ring-like features are starting to form in the lower-energy bands, shown in (e).

the First Animation, but resolved into the energy-bands of the slow, intermediate and fast fluctuations.

The picture which emerges is of a “three-speed” spin liquid. The slowest fluctuations (panel on left) exhibit the behaviour expected of the “spiral spin liquid”, with spins ferromagnetically aligned on the individual triangular plaquettes of the lattice, and exhibiting slow, collective rotations. Meanwhile the intermediate fluctuations (central panel), and fast fluctuations (panel on right), show a very different character. Spins are antiferromagnetically correlated on triangular plaquettes, and overlaid with a fast, correlated, single spin-flip dynamics redolent of the “weather vane” modes in Kagome lattice-antiferromagnets [38]. Fluctuations on different timescales can best be compared by adjusting the frame rate so as to approximately match the speeds of fluctuations in each panel (second half of the Second Animation [37]). Viewed in this way, we obtain a real-space picture of the very different correlations resolved in the partially-integrated structure factors shown in Fig. 7c,d, and in Fig. 7e.

DISCUSSION

The semi-classical simulations described in this Article provide a good account of many of the features observed in experiments on $\text{Ca}_{10}\text{Cr}_7\text{O}_{28}$, and paint a colourful picture of a spin liquid existing on multiple timescales. Just how un-

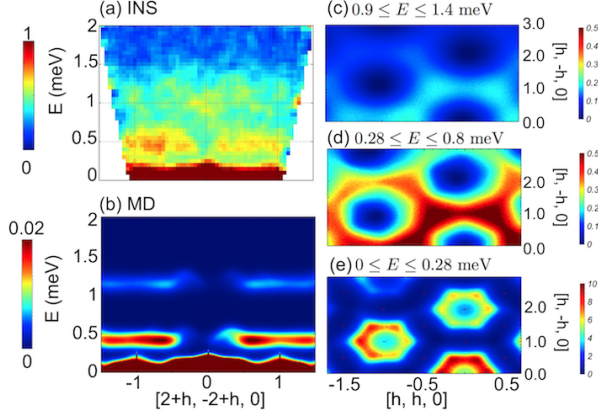


Figure 6. **Spin excitations of $\text{Ca}_{10}\text{Cr}_7\text{O}_{28}$ at the critical value of magnetic field ($B = 1$ T).** (a) Spin excitations measured in inelastic neutron scattering [17], integrated over $\Delta\mathbf{q} = \pm 0.2$ rlu perpendicular to the cut in reciprocal space. (b) Equivalent results from molecular dynamics (MD) simulations of \mathcal{H}_{BBK} [Eq. (1)], with parameters taken from experiment [Table I]. (c)–(e) Contribution to the energy-integrated structure factor $S(\mathbf{q})$ coming from excitations in the higher-, intermediate- and lower-energy bands visible in (b), within MD simulation. The gap to spin transverse spin excitations has closed, marking the onset of the low-field spin-liquid regime. This is characterised by a well-formed ring of correlations in $S(\mathbf{q})$, coming from spin excitations with low energy.

usual is this? Everyday life teaches that ordinary substances can have very different properties, depending on how long you wait. Water, the liquid which holds the key to life, acts like a solid in sudden impacts. Ice, meanwhile, is a solid which flows like a liquid over glacial timescales. Quantum systems too, hold many such surprises. In the quasi-one dimensional, quantum spin-ladder CaCu_2O_3 , static magnetic order coexists with high-energy spinon excitations [39]. Meanwhile, in the three-dimensional frustrated magnet $\text{Nd}_2\text{Zr}_2\text{O}_7$, all-in, all-out order coexists with excitations which support spin-ice like pinch points [40, 41], an effect which has been dubbed “moment fragmentation” [42]. $\text{Ca}_{10}\text{Cr}_7\text{O}_{28}$ appears to be unique, however, in having properties which resemble one spin liquid at low energies, and a different kind of spin liquid at higher energies.

This separation of timescales is relatively easy to visualise at a semi-classical level (cf. Second Animation [37]). However, this level of approximation neglects all entanglement between spins. To the best of our knowledge, this type of dynamics have yet to be explored for an entangled, fully-quantum system. So an important “next step” in the understanding of $\text{Ca}_{10}\text{Cr}_7\text{O}_{28}$ will be more, explicitly quantum, analysis of \mathcal{H}_{BBK} [Eq. (1)].

In this respect, there are a great many interesting, open, questions. We have argued that the key to understanding the low-energy properties of $\text{Ca}_{10}\text{Cr}_7\text{O}_{28}$ is the closing of a gap to a (quasi-)degenerate ring of spin excitations at $B = 1$ T. A scenario for such a phase transition has been previously dis-

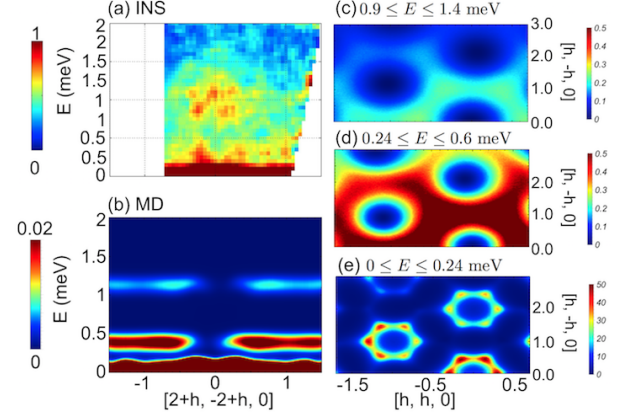


Figure 7. **Spin excitations of $\text{Ca}_{10}\text{Cr}_7\text{O}_{28}$ in the absence of magnetic field ($B = 0$ T).** (a) Spin excitations measured in inelastic neutron scattering [17], integrated over $\Delta\mathbf{q} = \pm 0.2$ rlu perpendicular to the cut in reciprocal space. (b) Equivalent results from molecular dynamics (MD) simulations of \mathcal{H}_{BBK} [Eq. (1)], with parameters taken from experiment [Table I]. (c)–(e) Contribution to the energy-integrated structure factor $S(\mathbf{q})$ coming from excitations in the higher-, intermediate- and lower-energy bands visible in (b), within MD simulation.

cussed by Sedrakyan and coauthors, who dubbed the degenerate ring of bosonic excitations a “moat-band” [43]. Considering the specific example of an XY model on the honeycomb lattice, with competing AF first- and second-neighbour interactions, they argued the ground state should be a chiral spin liquid, breaking inversion as well as time-reversal symmetries [44]. In this picture, excitations have the character of Fermions, and it could be interesting to try to model the low-energy properties of $\text{Ca}_{10}\text{Cr}_7\text{O}_{28}$ in terms of Fermionic quasiparticles. The existence of (Fermionic) fractional spin-excitations is also one possible explanation for a feature of the INS data which is not well-captured by semi-classical simulations, namely a broad continuum of “background” scattering extending up to ~ 1.5 meV for $B = 0$ T [cf. Fig. 7].

The high-energy and high-field properties of $\text{Ca}_{10}\text{Cr}_7\text{O}_{28}$ also pose interesting new questions for theory. The presence of competing FM and AF interactions immediately raises the possibility of magnons forming bound states, leading to a phase with hidden, multipolar order [45–47]. And the longitudinal fluctuations found in MD simulations (see Supplementary Information) provide at least a hint that spin waves are not the only excitations for $B > 1$ T. The presence of Kagome-like physics at high energy is also worth exploring in a quantum model, given the good agreement between semi-classical simulation and experiment. The pinch-point structures found at high energy, in high magnetic field, also have an interesting story to tell, with close parallels to work on $\text{Nd}_2\text{Zr}_2\text{O}_7$ [41]. An analytic theory of this phenomenon will be developed else-

where [36].

Further experiment would also be very helpful in unraveling the mysteries of $\text{Ca}_{10}\text{Cr}_7\text{O}_{28}$. The simulations described in this Article makes explicit predictions for the structure, and magnetic-field evolution, of inelastic neutron scattering which remain to be tested. Here polarisation-analysis could be a vital new ingredient, both to separate the magnetic signal from incoherent background in zero magnetic field, and to resolve the different transverse and longitudinal excitations in magnetic field [cf. Fig. 2, Supplemental Information]. Thermodynamic and transport measurements of $\text{Ca}_{10}\text{Cr}_7\text{O}_{28}$, which probe the low-energy excitations of its QSL ground state, could also be revealing. And given that $\text{Ca}_{10}\text{Cr}_7\text{O}_{28}$ may be proximate to an AF Kagome-like pump-probe experiments, for example using fast optics, might be particularly interesting.

Finally, since completing this work, we have become aware of a parallel study of $\text{Ca}_{10}\text{Cr}_7\text{O}_{28}$, by Biswas and Damle [48]. Their preprint provides a complementary analysis of the low-energy properties of \mathcal{H}_{HCM} [Eq. (2)], in the absence of magnetic field, and specifically addresses a question which we have not attempted to answer here, namely the fate of classical spins at temperatures $T \lesssim 60$ mK.

CONCLUSIONS

$\text{Ca}_{10}\text{Cr}_7\text{O}_{28}$ is a remarkable magnet, in which spin- $1/2$ Cr^{5+} ions form a bilayer breathing-kagome (BBK) lattice with complex, competing exchange interactions [19]. A combination of heat-capacity, magnetization, μSR , neutron-scattering, and AC susceptibility experiments reveal $\text{Ca}_{10}\text{Cr}_7\text{O}_{28}$ to be a gapless quantum spin liquid (QSL), showing no sign of magnetic order down to 19 mK [17, 18]. This spin liquid is characterised by spin fluctuations which show qualitatively different character on different timescales.

To better understand the nature and origin of the spin liquid in $\text{Ca}_{10}\text{Cr}_7\text{O}_{28}$, we have carried out large-scale semi-classical molecular-dynamics (MD) simulations of the minimal model of $\text{Ca}_{10}\text{Cr}_7\text{O}_{28}$, a Heisenberg model on the BBK lattice, with parameters taken from experiment [17, 18]. These simulations reveal a state where spins continue to fluctuate at very low temperatures, but the character of these fluctuations depends strongly on the timescale on which the dynamics are resolved, as shown in the Animations [27, 37].

We identify fluctuations at low energies with a “spiral spin liquid”, characterised by a ring of scattering in \mathbf{q} -space, and formed when the gap to a (quasi-)degenerate set of excitations closes at $B = 1$ T [cf. Fig. 3]. This spiral spin liquid can be described by an effective spin- $3/2$ Heisenberg model on a honeycomb lattice, formed by spin- $1/2$ moments on the triangular plaquettes of the BBK lattice in $\text{Ca}_{10}\text{Cr}_7\text{O}_{28}$ [cf. Fig. 2a, Fig. 2b]. The FM correlations of spins within these plaquettes are evident in the collective motion resolved at low energy in MD simulation (cf. Second Animation [37]).

Meanwhile, fluctuations at higher energy inherit their

character from the kagome-lattice antiferromagnet, and for $B > 1$ T, are characterised by sharp pinch-points in scattering [Fig. 4, Fig. 5]. These pinch points are encoded in spin fluctuations transverse to the applied magnetic field [cf. Fig. S2 of Supplemental Information], and can be resolved in MD simulations as collective rotations of antiferromagnetically correlated spins on shorter timescales (cf. Second Animation [37]). When the gap to transverse spin excitations closes, at $B = 1$ T, pinch points merge with excitations in the longitudinal channel to give rise to the broader “bow-tie” features observed in inelastic neutron scattering at higher energy [cf. Fig. 1].

These simulations capture many of the features of $\text{Ca}_{10}\text{Cr}_7\text{O}_{28}$; correctly reproducing the value of the critical field, $B = 1$ T [17, 18]; providing insight into the different structures seen in inelastic neutron scattering [17, 18]; and resolving the origin of the ring features found in Pseudo-Fermion Functional Renormalisation group (PFFRG) calculations [17]. To the best of our knowledge, they also provide the first theoretical example of a system which behaves like different types of spin liquid on different timescales.

Given this disparity of behaviour, it is tempting to ask just how many spin liquids there are in $\text{Ca}_{10}\text{Cr}_7\text{O}_{28}$? Since a quantum system should have one, unique, ground state, at low temperature the answer to this question must, ultimately, be: “one”. None the less, the success of semi-classical simulations in describing experiment suggests that this one ground state must incorporate two different types of correlations; one described by effective spin- $3/2$ moments on a honeycomb lattice; and one corresponding to antiferromagnetic fluctuations of individual spin- $1/2$ moments on a bilayer breathing-Kagome lattice. Unraveling the properties of this single, massively-entangled QSL, represents an exciting challenge for theory and experiment alike.

REFERENCES

-
- * rico.pohle@oist.jp
 - † han.yan@oist.jp
 - ‡ nic.shannon@oist.jp
 - [1] Leon Balents, “Spin liquids in frustrated magnets,” *Nature* **464**, 199–208 (2010).
 - [2] P. W. Anderson, “Resonating valence bonds: A new kind of insulator?” *Materials Research Bulletin* **8**, 153–160 (1973).
 - [3] Patrick A. Lee, “An end to the drought of quantum spin liquids,” *Science* **321**, 1306–1307 (2008), <http://science.sciencemag.org/content/321/5894/1306.full.pdf>.
 - [4] Y. Shimizu, K. Miyagawa, K. Kanoda, M. Maesato, and G. Saito, “Spin Liquid State in an Organic Mott Insulator with a Triangular Lattice,” *Phys. Rev. Lett.* **91**, 107001 (2003).
 - [5] Ryuichi Masutomi, Yoshitomo Karaki, and Hidehiko Ishimoto, “Gapless Spin Liquid Behavior in Two-Dimensional Solid ^3He ,” *Phys. Rev. Lett.* **92**, 025301 (2004).

- [6] Tian-Heng Han, Joel S. Helton, Shaoyan Chu, Daniel G. Nocera, Jose A. Rodriguez-Rivera, Collin Broholm, and Young S. Lee, “Fractionalized excitations in the spin-liquid state of a kagome-lattice antiferromagnet,” *Nature* **492**, 406–410 (2012).
- [7] Alexei Kitaev, “Anyons in an exactly solved model and beyond,” *Annals of Physics* **321**, 2 – 111 (2006), january Special Issue.
- [8] G. Jackeli and G. Khaliullin, “Mott insulators in the strong spin-orbit coupling limit: From heisenberg to a quantum compass and kitaev models,” *Phys. Rev. Lett.* **102**, 017205 (2009).
- [9] A. Banerjee, C. A. Bridges, J. Q. Yan, A. A. Aczel, L. Li, M. B. Stone, G. E. Granroth, M. D. Lumsden, Y. Yiu, J. Knolle, S. Bhattacharjee, D. L. Kovrizhin, R. Moessner, D. A. Tennant, D. G. Mandrus, and S. E. Nagler, “Proximate kitaev quantum spin liquid behaviour in a honeycomb magnet,” *Nat. Mater.* **15**, 733–740 (2016).
- [10] S.-H. Baek, S.-H. Do, K.-Y. Choi, Y. S. Kwon, A. U. B. Wolter, S. Nishimoto, Jeroen van den Brink, and B. Büchner, “Evidence for a Field-Induced Quantum Spin Liquid in α -RuCl₃,” *Phys. Rev. Lett.* **119**, 037201 (2017).
- [11] Michael Hermele, Matthew P. A. Fisher, and Leon Balents, “Pyrochlore photons: The U(1) spin liquid in a $S=\frac{1}{2}$ three-dimensional frustrated magnet,” *Phys. Rev. B* **69**, 064404 (2004).
- [12] Argha Banerjee, Sergei V. Isakov, Kedar Damle, and Yong Baek Kim, “Unusual liquid state of hard-core bosons on the pyrochlore lattice,” *Phys. Rev. Lett.* **100**, 047208 (2008).
- [13] Owen Benton, Olga Sikora, and Nic Shannon, “Seeing the light: Experimental signatures of emergent electromagnetism in a quantum spin ice,” *Phys. Rev. B* **86**, 075154 (2012).
- [14] Romain Sibille, Nicolas Gauthier, Han Yan, Monica Ciomaga Hatnean, Jacques Ollivier, Barry Winn, Geetha Balakrishnan, Michel Kenzelmann, Nic Shannon, and Tom Fennell, “Experimental signatures of emergent quantum electrodynamics in a quantum spin ice,” [arXiv:1706.03604](https://arxiv.org/abs/1706.03604).
- [15] Iztok Arcon, Breda Mirtic, and Alojz Kodre, “Determination of valence states of chromium in calcium chromates by using x-ray absorption near-edge structure (xanes) spectroscopy,” *Journal of the American Ceramic Society* **81**, 222–224 (1998).
- [16] Dalma Gyepesová and Vratislav Langer, “Ca₁₀(Cr^VO₄)₆(Cr^VO₄), a disordered mixed-valence chromium compound exhibiting inversion twinning,” *Acta Crystallographica Section C* **69**, 111–113 (2013).
- [17] Christian Balz, Bella Lake, Johannes Reuther, Hubertus Luetkens, Rico Schonemann, Thomas Hermannsdorfer, Yogesh Singh, A. T. M. Nazmul Islam, Elisa M. Wheeler, Jose A. Rodriguez-Rivera, Tatiana Guidi, Giovanna G. Simeoni, Chris Baines, and Hanjo Ryll, “Physical realization of a quantum spin liquid based on a complex frustration mechanism,” *Nat. Phys.* **12**, 942–949 (2016).
- [18] Christian Balz, Bella Lake, A. T. M. Nazmul Islam, Yogesh Singh, Jose A. Rodriguez-Rivera, Tatiana Guidi, Elisa M. Wheeler, Giovanna G. Simeoni, and Hanjo Ryll, “Magnetic Hamiltonian and phase diagram of the quantum spin liquid Ca₁₀Cr₇O₂₈,” *Phys. Rev. B* **95**, 174414 (2017).
- [19] Christian Balz, Bella Lake, Manfred Reehuis, A T M Nazmul Islam, Oleksandr Prokhnenko, Yogesh Singh, Philip Pattison, and Sándor Tóth, “Crystal growth, structure and magnetic properties of Ca₁₀Cr₇O₂₈,” *Journal of Physics: Condensed Matter* **29**, 225802 (2017).
- [20] D. L. Quintero-Castro, B. Lake, E. M. Wheeler, A. T. M. N. Islam, T. Guidi, K. C. Rule, Z. Izaola, M. Russina, K. Kiefer, and Y. Skourski, “Magnetic excitations of the gapped quantum spin dimer antiferromagnet Sr₃Cr₂O₈,” *Phys. Rev. B* **81**, 014415 (2010).
- [21] Zhe Wang, D. L. Quintero-Castro, S. Zherlitsyn, S. Yasin, Y. Skourski, A. T. M. N. Islam, B. Lake, J. Deisenhofer, and A. Loidl, “Field-Induced Magnonic Liquid in the 3D Spin-Dimerized Antiferromagnet Sr₃Cr₂O₈,” *Phys. Rev. Lett.* **116**, 147201 (2016).
- [22] E. Rastelli, A. Tassi, and L. Reatto, “Non-simple magnetic order for simple Hamiltonians,” *Physica B+C* **97**, 1–24 (1979).
- [23] J.B. Fouet, P. Sindzingre, and C. Lhuillier, “An investigation of the quantum $J_1 - J_2 - J_3$ model on the honeycomb lattice,” *The European Physical Journal B - Condensed Matter and Complex Systems* **20**, 241–254 (2001).
- [24] R. Moessner and J. T. Chalker, “Properties of a Classical Spin Liquid: The Heisenberg Pyrochlore Antiferromagnet,” *Phys. Rev. Lett.* **80**, 2929–2932 (1998).
- [25] P. H. Conlon and J. T. Chalker, “Absent pinch points and emergent clusters: Further neighbor interactions in the pyrochlore Heisenberg antiferromagnet,” *Phys. Rev. B* **81**, 224413 (2010).
- [26] Mathieu Taillefumier, Julien Robert, Christopher L. Henley, Roderich Moessner, and Benjamin Canals, “Semiclassical spin dynamics of the antiferromagnetic Heisenberg model on the kagome lattice,” *Phys. Rev. B* **90**, 064419 (2014).
- [27] “Animation of spin dynamics of Ca₁₀Cr₇O₂₈ in zero magnetic field,” Supplementary Material.
- [28] Soichiro Okumura, Hikaru Kawamura, Tsuyoshi Okubo, and Yukitoshi Motome, “Novel Spin-Liquid States in the Frustrated Heisenberg Antiferromagnet on the Honeycomb Lattice,” *Journal of the Physical Society of Japan* **79**, 114705 (2010).
- [29] Luis Seabra, Philippe Sindzingre, Tsutomu Momoi, and Nic Shannon, “Novel phases in a square-lattice frustrated ferromagnet: $\frac{1}{3}$ -magnetization plateau, helicoidal spin liquid, and vortex crystal,” *Phys. Rev. B* **93**, 085132 (2016).
- [30] Doron Bergman, Jason Alicea, Emanuel Gull, Simon Trebst, and Leon Balents, “Order-by-disorder and spiral spin-liquid in frustrated diamond-lattice antiferromagnets,” *Nat Phys* **3**, 487–491 (2007).
- [31] P. Chandra and B. Doucot, “Possible spin-liquid state at large S for the frustrated square Heisenberg lattice,” *Phys. Rev. B* **38**, 9335–9338 (1988).
- [32] Smerald, A. and Shannon, N., “The double life of electrons in magnetic iron pnictides as revealed by nmr,” *EPL* **92**, 47005 (2010).
- [33] D. A. Garanin and Benjamin Canals, “Classical spin liquid: Exact solution for the infinite-component antiferromagnetic model on the kagomé lattice,” *Phys. Rev. B* **59**, 443–456 (1999).
- [34] M. E. Zhitomirsky, “Octupolar ordering of classical kagome antiferromagnets in two and three dimensions,” *Phys. Rev. B* **78**, 094423 (2008).
- [35] Christopher L. Henley, “The “coulomb phase” in frustrated systems,” *Annual Review of Condensed Matter Physics* **1**, 179–210 (2010).
- [36] H. Yan, R. Pohle, and N. Shannon, in preparation.
- [37] “Animation of spin dynamics of Ca₁₀Cr₇O₂₈ in zero magnetic field, resolved into different bands of excitations,” Supplementary Material.
- [38] A. B. Harris, C. Kallin, and A. J. Berlinsky, “Possible Néel orderings of the Kagomé antiferromagnet,” *Phys. Rev. B* **45**, 2899–2919 (1992).
- [39] Bella Lake, Alexei M. Tsvelik, Susanne Notbohm, D. Alan Tennant, Toby G. Perring, Manfred Reehuis, Chinnathambi Sekar, Gernot Krabbes, and Bernd Buchner, “Confinement of fractional quantum number particles in a condensed-matter system,” *Nat Phys* **6**, 50–55 (2010).
- [40] S. Petit, E. Lhotel, B. Canals, M. Ciomaga Hatnean, J. Ollivier,

- H. Mutka, E. Ressouche, A. R. Wildes, M. R. Lees, and G. Balakrishnan, “Observation of magnetic fragmentation in spin ice,” *Nat Phys* **12**, 746–750 (2016).
- [41] Owen Benton, “Quantum origins of moment fragmentation in $\text{Nd}_2\text{Zr}_2\text{O}_7$,” *Phys. Rev. B* **94**, 104430 (2016).
- [42] M. E. Brooks-Bartlett, S. T. Banks, L. D C Jaubert, A. Harman-Clarke, and P. C W Holdsworth, “Magnetic-Moment Fragmentation and Monopole Crystallization,” *Phys. Rev. X* **4**, 011007 (2014).
- [43] Tigran A. Sedrakyan, Leonid I. Glazman, and Alex Kamenev, “Absence of bose condensation on lattices with moat bands,” *Phys. Rev. B* **89**, 201112 (2014).
- [44] Tigran A. Sedrakyan, Leonid I. Glazman, and Alex Kamenev, “Spontaneous formation of a nonuniform chiral spin liquid in a moat-band lattice,” *Phys. Rev. Lett.* **114**, 037203 (2015).
- [45] Andrey V. Chubukov, “Chiral, nematic, and dimer states in quantum spin chains,” *Phys. Rev. B* **44**, 4693–4696 (1991).
- [46] Nic Shannon, Tsutomu Momoi, and Philippe Sindzingre, “Nematic Order in Square Lattice Frustrated Ferromagnets,” *Phys. Rev. Lett.* **96**, 027213 (2006).
- [47] Tsutomu Momoi, Philippe Sindzingre, and Nic Shannon, “Octupolar order in the multiple spin exchange model on a triangular lattice,” *Phys. Rev. Lett.* **97**, 257204 (2006).
- [48] S. Biswas and K. Damle, “Semiclassical theory for liquid-like behaviour of the frustrated magnet $\text{Ca}_{10}\text{Cr}_7\text{O}_{28}$,” [arXiv:1707.04834v1](https://arxiv.org/abs/1707.04834).
- [49] J. A. Olive, A. P. Young, and D. Sherrington, “Computer simulation of the three-dimensional short-range heisenberg spin glass,” *Phys. Rev. B* **34**, 6341–6346 (1986).
- [50] Y Miyatake, M Yamamoto, J J Kim, M Toyonaga, and O Nagai, “On the implementation of the ‘heat bath’ algorithms for monte carlo simulations of classical heisenberg spin systems,” *Journal of Physics C: Solid State Physics* **19**, 2539 (1986).
- [51] Robert H. Swendsen and Jian-Sheng Wang, “Replica monte carlo simulation of spin-glasses,” *Phys. Rev. Lett.* **57**, 2607–2609 (1986).
- [52] David J. Earl and Michael W. Deem, “Parallel tempering: Theory, applications, and new perspectives,” *Phys. Chem. Chem. Phys.* **7**, 3910–3916 (2005).
- [53] Michael Creutz, “Overrelaxation and monte carlo simulation,” *Phys. Rev. D* **36**, 515–519 (1987).
- [54] William H. Press, Saul A. Teukolsky, William T. Vetterling, and Brian P. Flannery, *Numerical Recipes 3rd Edition: The Art of Scientific Computing*, 3rd ed. (Cambridge University Press, New York, NY, USA, 2007).
- [55] Ernst Hairer, Gerhard Wanner, and Syvert P. Nørsett, *Solving Ordinary Differential Equations I – Nonstiff Problems* (Springer Berlin Heidelberg, 1993).
- [56] Matteo Frigo and Steven G. Johnson, “The design and implementation of FFTW3,” *Proceedings of the IEEE* **93**, 216–231 (2005), special issue on “Program Generation, Optimization, and Platform Adaptation”.
- [57] George B. Arfken and Hans J. Weber, *Mathematical Methods for Physicists – International Edition*, 4th ed. (Academic Press, INC, 1995).
- [58] A. J. Dianoux and G. Lander, “Neutron data booklet,” ISBN: 0-9704143-7-4.
- [59] C. Balz, “Private communication.”

ACKNOWLEDGEMENTS

The authors are pleased to acknowledge helpful conversations with Owen Benton, Ludovic Jaubert and Mathieu TAILLIEUMIER, and are indebted to Christian Balz and Bella Lake for extended discussions and sharing information about experiments on $\text{Ca}_{10}\text{Cr}_7\text{O}_{28}$. The authors also gratefully acknowledge help with data visualization, provided by Pavel Puchenkov, of the Scientific Computing and Data Analysis Section, OIST. This work was supported by the Theory of Quantum Matter Unit, OIST. Numerical calculations we carried out using HPC Facilities provided by OIST.

AUTHOR CONTRIBUTIONS

Both RP and HY contributed equally to this work and have been listed in alphabetical order. RP carried out all numerical simulations, and analysis of numerical and experimental data. HY initiated the project and carried out parallel analytic calculations. NS supervised the project, and prepared the manuscript, with input from HY and RP.

METHODS

Monte Carlo Simulation: All of the results presented in this Article are based on spin configurations drawn from classical Monte Carlo simulations of \mathcal{H}_{BBK} [Eq. (1)]. Monte Carlo simulations were performed by using a local heat-bath algorithm [49, 50], in combination with parallel tempering [51, 52], and over-relaxation techniques [53]. A single MC step consists of N local heat-bath updates on randomly chosen sites, and two over-relaxation steps, each comprising a π -rotation of all the spins in the lattice about their local exchange fields. Simulations were performed in parallel for replicas at 200 different temperatures, with replica-exchange initiated by the parallel tempering algorithm every 10^2 MC steps. Results for thermodynamic quantities were averaged over 10^6 statistically independent samples, after initial 10^6 MC steps for simulated annealing and 10^6 MC steps for thermalisation. All presented results have been calculated for clusters of $N = 13824$ sites.

Molecular Dynamics (MD) Simulation: Our MD simulations are based on the semi-classical, Heisenberg equations of motion

$$\frac{d\mathbf{S}_i}{dt} = \frac{i}{\hbar} [\mathcal{H}_{\text{BBK}}, \mathbf{S}_i] = \left(\sum_j J_{ij} \mathbf{S}_j - \mathbf{B} \right) \times \mathbf{S}_i, \quad (3)$$

where j accounts for all nearest-neighbouring sites of i and J_{ij} is given in Table I. Numerical integration of Eq. (3) was carried out using a 4th order Runge-Kutta algorithm, as described in [54, 55]. Spin configurations for MD simulation were taken from the thermal ensemble generated by classical MC simulations of \mathcal{H}_{BBK} at $T = 222$ mK, for parameters

taken from experiment (cf. Table I). The dynamical structure factor

$$S(\mathbf{q}, \omega) = \frac{1}{\sqrt{N_t N}} \sum_{i,j}^N e^{i\mathbf{q}(\mathbf{r}_i - \mathbf{r}_j)} \sum_n^{N_t} e^{i\omega n \delta t} \langle \mathbf{S}_i(0) \cdot \mathbf{S}_j(t) \rangle, \quad (4)$$

was calculate using Fast Fourier Transform (FFT) [56], and averaged over spin dynamics obtained from 1000 independent initial spin configurations. MD simulations were performed for $N_t = 600$ time steps, with the time-increment δt of

$$\delta t = \frac{t_{\max}}{N_t} = \frac{2\pi}{\omega_{\max}} \quad (5)$$

and a maximally resolvable frequency limit of $\omega_{\max} = 6$ meV. To avoid numerical artefacts (Gibbs phenomenon [57]) coming from discontinuities of the finite time-window, at $t = 0$ and $t = t_{\max}$, the time sequence of spin configurations has been multiplied by a Gaussian envelop, imposing a Gaussian energy resolution of FWHM ≈ 0.03 meV, on the numerically-obtained $S(\mathbf{q}, \omega)$ [see Supplementary Information for further details].

Comparison with Experiment: Predictions for inelastic neutron scattering are plotted as

$$\frac{d^2\sigma}{d\Omega dE_f} \propto I(\mathbf{q}, \omega) \quad (6)$$

where we calculate

$$I(\mathbf{q}, \omega) = \mathcal{F}(\mathbf{q})^2 \sum_{\alpha, \beta} \left(\delta_{\alpha\beta} - \frac{q_\alpha q_\beta}{\mathbf{q}^2} \right) S^{\alpha\beta}(\mathbf{q}, \omega). \quad (7)$$

Here $\mathcal{F}(\mathbf{q})$ is the atomic form factor appropriate to a Cr^{5+} ion, and following [58], we write

$$\mathcal{F}(\mathbf{q}) = \langle j_0(\mathbf{q}) \rangle + \left(1 - \frac{2}{g} \right) \langle j_2(\mathbf{q}) \rangle. \quad (8)$$

We consider gyromagnetic ratio $g = 2$, implying that $\langle j_2(\mathbf{q}) \rangle$ plays no role. The remaining function, $\langle j_0(\mathbf{q}) \rangle$ can be parameterised as

$$\langle j_0(\mathbf{q}) \rangle = A e^{-a(|\mathbf{q}|/4\pi)^2} + B e^{-b(|\mathbf{q}|/4\pi)^2} + C e^{-c(|\mathbf{q}|/4\pi)^2} + D. \quad (9)$$

where, be consistent with earlier work [59], coefficients are taken to be

$$A = -0.2602, \quad B = 0.33655, \quad C = 0.90596, \quad D = 0.0159 \quad (10)$$

$$a = 0.03958, \quad b = 15.24915, \quad c = 3.2568. \quad (11)$$

For comparison with experiment, following [17, 18], MD results for $S(\mathbf{q}, \omega)$ have further been convoluted in energy with a Gaussian of FWHM = 0.2 meV.

Supplementary Material : How many spin liquids are there in $\text{Ca}_{10}\text{Cr}_7\text{O}_{28}$?

Rico Pohle,^{1,*} Han Yan,^{1,†} and Nic Shannon¹

¹*Okinawa Institute of Science and Technology Graduate University, Onna-son, Okinawa 904-0412, Japan*
(Dated: November 10, 2017)

* rico.pohle@oist.jp
† han.yan@oist.jp

ANIMATIONS OF MOLECULAR DYNAMICS SIMULATIONS

First Animation

In the First Animation, we show a “fly through” of spins on the breathing bilayer Kagome (BBK) lattice, with time evolution taken from a single molecular dynamics (MD) simulation of \mathcal{H}_{BBK} [Eq. (1)], for parameters relevant to $\text{Ca}_{10}\text{Cr}_7\text{O}_{28}$ [Table 1 of the main text]. The simulation was carried out for a cluster of $N = 5400$ sites, at a temperature of $T = 222\text{mK}$. The total number of time steps in the simulation was $N_t = 6000$, and in order to obtain a smooth rotation of spins in the animation, the time step for each frame has been set to $\delta t \approx 0.1 \hbar^{-1}\text{meV}^{-1}$ [cf. Eq.(5) of the main text]. The animation was prepared using the open-source software package “Blender” [1]. To emphasize the dynamics on different timescales, spins have been color-coded according to their speed of rotation, with red indicating fast rotation, and green denoting slow rotation.

Second Animation

In the Second Animation we show results taken from a single MD simulation of \mathcal{H}_{BBK} , equivalent to that shown in the First Animation. However in this case, the time sequence for the spin dynamics has been separated into slow, intermediate and fast components, to emphasise the dynamics on different timescales. This is accomplished by first performing a fast Fourier transform (FFT) on the time sequence of each spin, then filtering the resulting signal in frequency space, using a digital analogue of a “band-pass” filter. The frequencies used for this band-pass filter are $0.750\text{--}1.500\text{ meV}$ (fast fluctuations); $0.225\text{--}0.750\text{ meV}$ (intermediate fluctuations); and $0.00\text{--}0.225\text{ meV}$ (slow fluctuations). After filtering in frequency, a second FFT is used to reconstruct separate time sequences for slow, intermediate and fast fluctuations. The final result for each of these is presented in the three panels of the Second Animation.

In the second part of the Second Animation, the speed of playback for three time sequences has been adjusted, so as to match the characteristic speed of the relevant fluctuations. To accommodate this, a much longer sequence of $N_t = 130000$ time steps has been generated from MD simulation, using a much shorter time increment of $\delta t \approx 0.035 \hbar^{-1}\text{meV}^{-1}$. The adjustment of playback speed has been accomplished within “Blender” [1], by adjusting the number of frames included for each time sequence. Viewed in this way, the very different dynamics on different timescales is self-evident. Intermediate and fast fluctuations show dynamics redolent of the Heisenberg antiferromagnet on the Kagome-lattice. Meanwhile, qualitatively different dynamics, corresponding to the “spiral spin liquid”, are resolved in the slow fluctuations of the spins. In all three cases, the dynamics is highly-localised, consistent with the weakly-dispersing bands of excitations resolved in MD results for $S(\mathbf{q}, \omega)$ [Fig. S1].

EVOLUTION OF SPIN DYNAMICS IN APPLIED MAGNETIC FIELD

In Fig. S1 we compare the field-evolution of spin excitations found in inelastic neutron scattering (INS) measurements of $\text{Ca}_{10}\text{Cr}_7\text{O}_{28}$ [2] with MD simulations of \mathcal{H}_{BBK} [Eq. (1) of the main text]. Results for experiment are shown in the first row of panels, Fig. S1a. Both experiment and simulations have been carried out at a temperature $T \approx 220\text{ mK}$.

So far as simulations are concerned, our main tool for understanding spin fluctuations is the dynamical structure factor $S(\mathbf{q}, \omega)$, defined in Eq. 4 of the main text. In the second row of the figure [Fig. S1b], we show predictions for experiment derived from $S(\mathbf{q}, \omega)$; following [2], for comparison with experiment, results have been convoluted with a Gaussian of FWHM = 0.2 meV , and weighted by the atomic form factor for Cr^{5+} , as described in the Methods section of the main text. These results provide an excellent account of all of the sharp features seen in experiment [Fig. S1a].

For comparison, in the third row [Fig. S1c], we show “raw” simulation results for a cluster of $N = 1944$ spins. These simulations have a native energy resolution of 0.015 meV , set by the length of the time-sequence, $N_t = 400$. Results have further been multiplied by a Gaussian envelope in time, to remove numerical artifacts coming from the finite extent of the time sequence. This is equivalent to a convolution with a Gaussian of FWHM = 0.04 meV in energy, to set a combined limit on the energy resolution of $\Delta\omega = 0.055\text{ meV}$. And, in order to compensate for a gradient in intensity $\propto T/\omega$, coming from classical thermodynamics, we do not plot the dynamical structure factor $S(\mathbf{q}, \omega)$ directly, but rather its first moment

$$\tilde{S}(\mathbf{q}, \omega) = \omega S(\mathbf{q}, \omega) . \quad (1)$$

Plotted in this way, excitations at intermediate and high energy exhibit similar spectral weight, and it is possible to identify individual bands of dispersing excitations, especially at high values of magnetic field.

It is also interesting to resolve the contributions to $S(\mathbf{q}, \omega)$ coming from transverse and longitudinal fluctuations, i.e.

$$S(\mathbf{q}, \omega) = S^\perp(\mathbf{q}, \omega) + S^\parallel(\mathbf{q}, \omega) \quad (2)$$

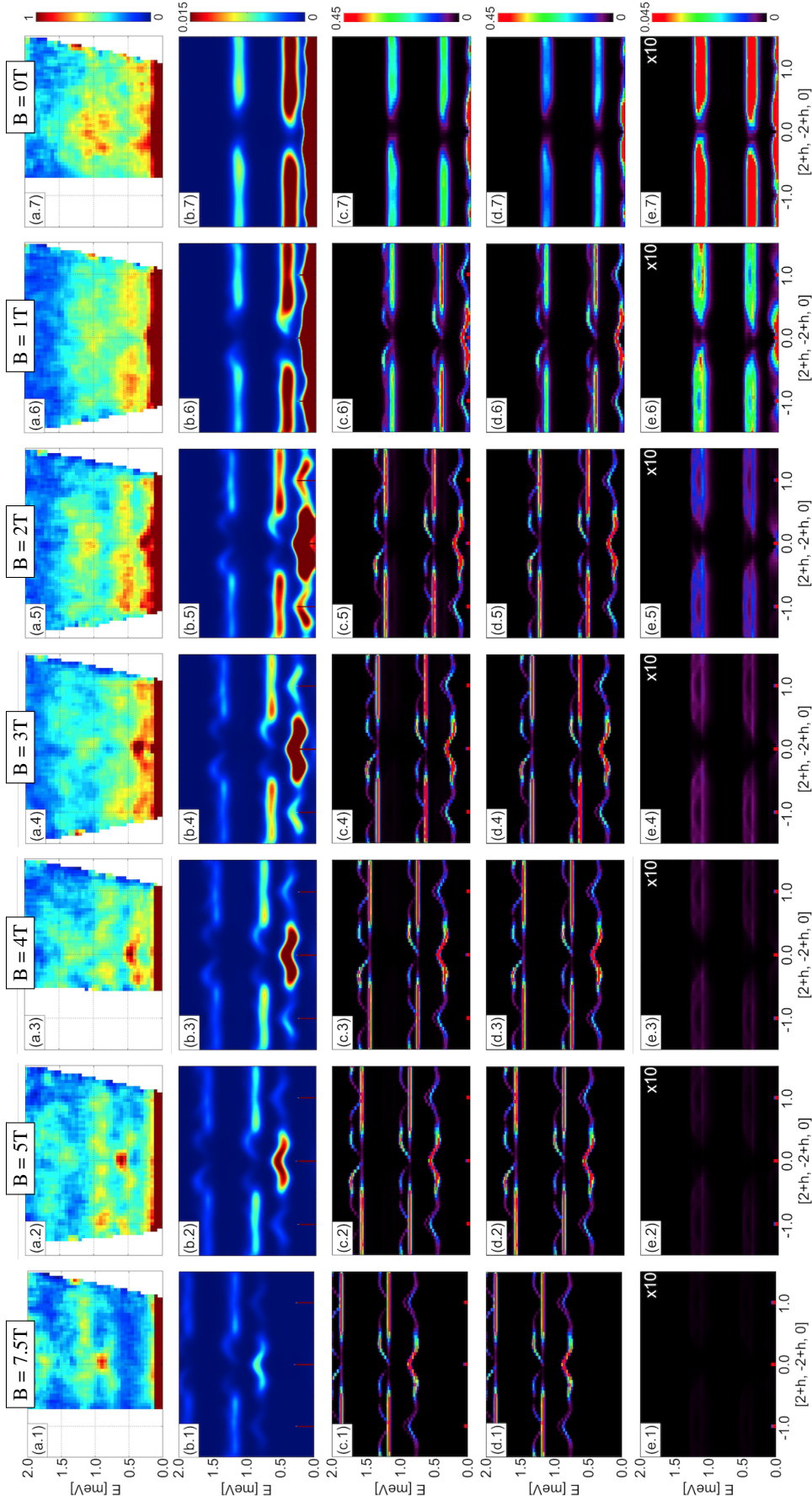


Figure 1. **Evolution of spin excitations as a function of magnetic field.** (a) Inelastic neutron scattering results for $\text{Ca}_{10}\text{Cr}_7\text{O}_{28}$, reproduced from [2], for magnetic fields ranging from $B = 7.5$ T to $B = 0$ T. (b) Predictions for inelastic scattering taken from MD simulations of \mathcal{H}_{BBK} , as described in the Methods section of the main text. (c) Simulation results for the first moment of the dynamical structure factor $\tilde{S}(\mathbf{q}, \omega)$ [Eq. (S1)]. (d) Contribution to $\tilde{S}(\mathbf{q}, \omega)$ coming from transverse spin fluctuations $\tilde{S}^{\perp}(\mathbf{q}, \omega)$ [Eq. (S5)]. (e) Contribution to $\tilde{S}(\mathbf{q}, \omega)$ coming from longitudinal spin fluctuations $\tilde{S}^{\parallel}(\mathbf{q}, \omega)$ [Eq. (S6)], multiplied $\times 10$. Further details of simulations can be found in the text.

where

$$S^\perp(\mathbf{q}, \omega) = \frac{1}{\sqrt{N_t}} \sum_n e^{i\omega n \delta t} \langle \mathbf{S}_\mathbf{q}^\perp(t) \cdot \mathbf{S}_{-\mathbf{q}}^\perp(0) \rangle, \quad \mathbf{S}_i^\perp = (S_i^x, S_i^y), \quad (3)$$

and

$$S^\parallel(\mathbf{q}, \omega) = \frac{1}{\sqrt{N_t}} \sum_n e^{i\omega n \delta t} \langle S_\mathbf{q}^z(t) \cdot S_{-\mathbf{q}}^z(0) \rangle. \quad (4)$$

In the fourth row [Fig. S1d], we plot results for the first moment of the dynamical structure factor for transverse excitations

$$\tilde{S}^\perp(\mathbf{q}, \omega) = \omega S^\perp(\mathbf{q}, \omega). \quad (5)$$

At high values of field, this clearly picks out six different branches spin-wave excitations, in correspondence with the results of linear spin-wave theory [2]. The gap to each of these excitations scales linearly with field, with the gap to the lowest lying transverse excitation closing for $B = 1$ T [cf. Fig. S3]. The intermediate and high-energy spin-wave branches are qualitatively similar, and both contain flat bands of localised spin-wave excitations, similar to those found in the Heisenberg antiferromagnet on the Kagome lattice [3–5].

Meanwhile, in the fifth row [Fig. S1d], we plot results for the first moment of the dynamical structure factor associated with longitudinal excitations

$$\tilde{S}^\parallel(\mathbf{q}, \omega) = \omega S^\parallel(\mathbf{q}, \omega). \quad (6)$$

The strongest signal in the longitudinal channel is an elastic peak in the zone-center, corresponding to the finite magnetisation of the system for $B > 0$ T. These are visible in Fig. 2h, but are eliminated here by the factor ω in Eq. (6).

Apart from the elastic signal, the spectral weight found in longitudinal channel becomes negligible for $B > 5$ T. However, at lower values of magnetic field, simulations also reveal three bands of highly-localised longitudinal excitations. The energy of these excitations does not depend on the value of magnetic field, and the lowest-lying longitudinal excitations are found to be gapless. The spectral weight found in all three bands grows as the magnetic field (and thereby the magnetisation) is reduced. The structure of these longitudinal excitations is discussed in more detail below.

DYNAMICAL STRUCTURE FACTORS AT $B = 2$ T

In Fig. 2 we compare MD results for transverse and longitudinal spin excitations found at a field of $B = 2$ T. Simulations were carried out at $T = 222$ mK, for parameters appropriate to $\text{Ca}_{10}\text{Cr}_7\text{O}_{28}$, as described in the main text. No attempt has been made to correct for the magnetic form factor of Cr^{5+} , experimental resolution, or the polarisation-dependence of scattering.

We first consider transverse excitations, as resolved in $S^\perp(\mathbf{q}, \omega)$ [Eq. (S3)]. For this value of field, it is still possible to resolve six distinct bands of spin-wave excitations, grouped into pairs at low, intermediate and high energy [Fig. S2(a)]. These exhibit flat bands at energies of $E = 0.54$ meV and $E = 1.23$ meV. At an energy of $\hbar\omega = 0.57$ meV (slightly above the lowest-lying flat band), results for $S^\perp(\mathbf{q}, \omega)$, reveal characteristic “half-moon” features near the zone centers, overlaid on a lattice of highly-structured “bow-tie” features [Fig. S2(c)]. The origin of these “half-moon” features, which are also observed in MD simulations of the Heisenberg antiferromagnet on a Kagome lattice [6], will be discussed elsewhere [7]. At an energy of $\hbar\omega = 0.54$ meV, the “bow-tie” features resolve into a set of zone-center pinch points, familiar from the Heisenberg antiferromagnet on a Kagome lattice [3–5] [Fig. S2(e)]. Very different structure is resolved in transverse fluctuations at an energy of $\hbar\omega = 0.135$ meV, where the rings, characteristic of a spiral spin liquid are clearly resolved [Fig. S2(g)]. The origin of these features is discussed at some length in the main text.

We now turn to longitudinal excitations, as resolved in simulation results for $S^\parallel(\mathbf{q}, \omega)$ [Eq. S4]. Like transverse spin fluctuations, these are naturally grouped into excitations at low, intermediate and high energy, which show little dispersion [Fig. S2(b)]. Cuts through $S^\parallel(\mathbf{q}, \omega)$ at intermediate energy reveal a network of broad features [Fig. S2(d) and Fig. S2(f)]. Results for high energy excitations (not shown) are very similar. But once again, results at low energy have a dramatically different character, with the majority of spectral weight found in elastic peaks in one quarter of the Brillouin zones, which interpolate through broad, diffuse, scattering to the BZ boundary [Fig. S2(h)].

FIELD EVOLUTION OF GAP TO TRANSVERSE SPIN EXCITATIONS

In Fig. S3 we show the field-evolution of the gap to the lowest-lying transverse spin excitations, extracted from MD simulation results for $S^\perp(\mathbf{q}, \omega)$ [cf. Fig. S1]. The gap, $\Delta(B)$, interpolates linearly to zero for $B \rightarrow 1.0(5)$ T. This result is consistent with changes in the form of the specific-heat $c(T)$ at $B = 1.0$ T, as reported by Balz *et al.* [2].

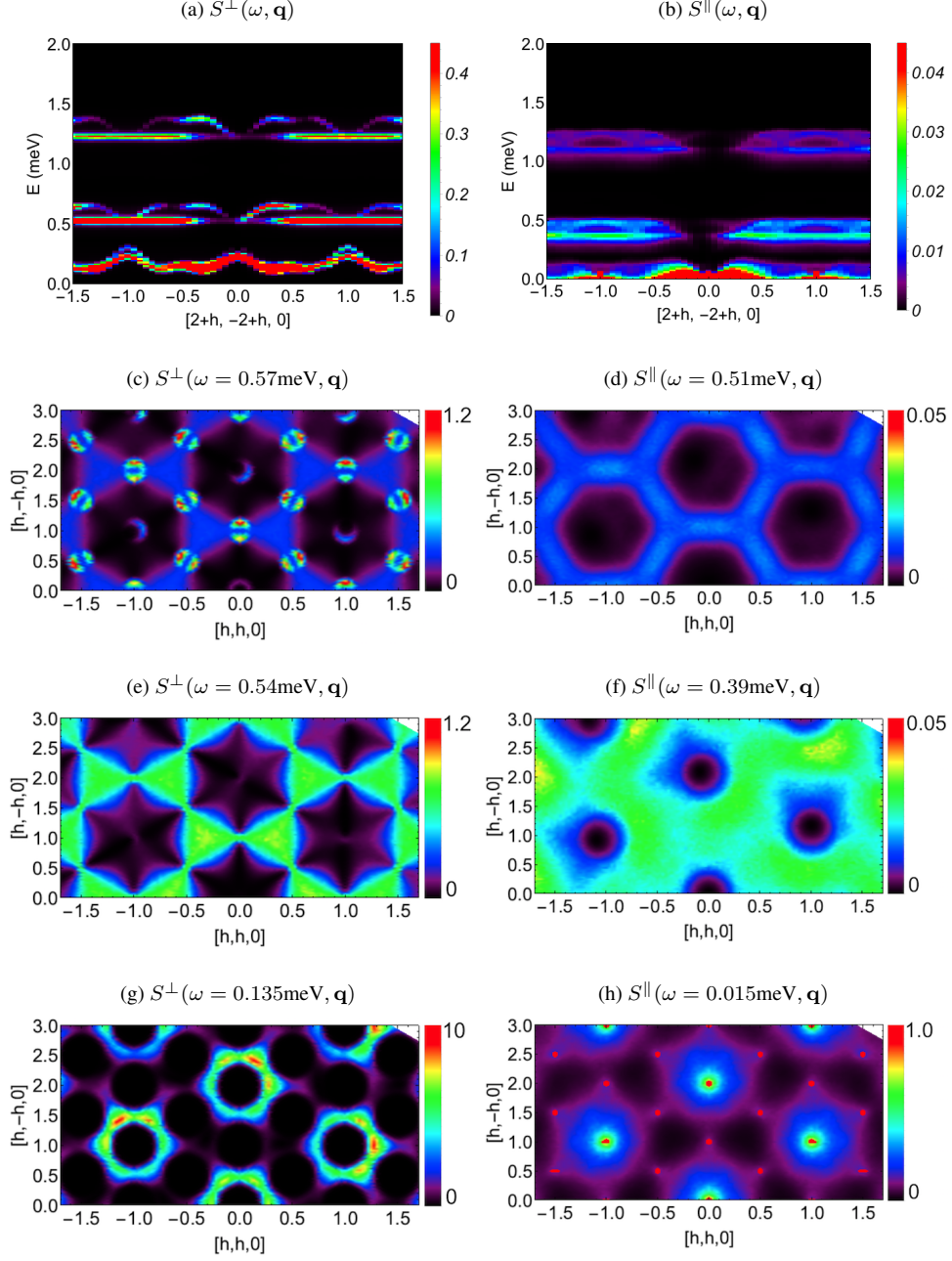


Figure 2. **Transverse and longitudinal spin excitations, as found in MD simulations at $B = 2$ T.** (a) Simulation results for the transverse structure factor $S^\perp(\mathbf{q}, \omega)$ [Eq. (3)], showing six distinct branches of spin-wave excitations. (b) Corresponding results for $S^\parallel(\mathbf{q}, \omega)$ [Eq. (4)], showing weakly-dispersing longitudinal spin excitations at three distinct energy scales. (c) $S^\perp(\mathbf{q}, \omega)$ at intermediate energy $\hbar\omega = 0.57$ meV, showing “half-moon” features overlaid on a lattice of “bow-tie” features. (d) $S^\parallel(\mathbf{q}, \omega)$ at intermediate energy $\hbar\omega = 0.51$ meV, showing a network of broad scattering. (e) $S^\perp(\mathbf{q}, \omega)$ at intermediate energy $\hbar\omega = 0.54$ meV, showing sharp “pinch-point” features. (f) $S^\parallel(\mathbf{q}, \omega)$ at intermediate energy $\hbar\omega = 0.39$ meV, showing evolution of the network of broad scattering. (g) $S^\perp(\mathbf{q}, \omega)$ at low energy $\hbar\omega = 0.135$ meV, showing the ring-feature associated with the spiral spin liquid. (h) $S^\parallel(\mathbf{q}, \omega)$ at low energy $\hbar\omega = 0.015$ meV, showing zone-center elastic peaks associated with finite magnetisation, and accompanying broad, diffuse scattering. All simulations were carried out at $T = 222$ mK, for parameters relevant to $\text{Ca}_{10}\text{Cr}_7\text{O}_{28}$. Further details of simulations can be found in the main text.

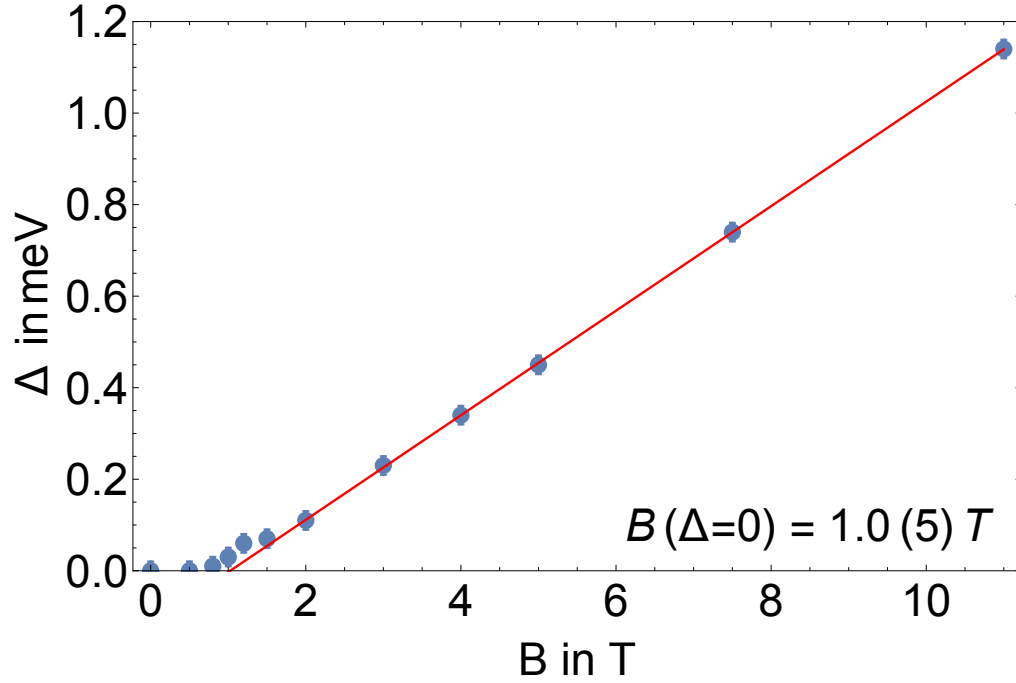


Figure 3. **Field evolution of gap to the lowest-lying transverse spin excitations, $\Delta(B)$.** MD simulations were carried out for parameters relevant to $\text{Ca}_{10}\text{Cr}_7\text{O}_{28}$, at a temperature of $T = 222$ mK, as described in the main text. The red line shows a linear regression of the data, with $\Delta(B) \rightarrow 0$ for $B = 1.0(5)$ T. Error bars on points reflect the finite energy resolution of MD results.

REFERENCES

-
- [1] “Blender open source animation software.” <http://www.blender.org>.
 - [2] Christian Balz, Bella Lake, A. T. M. Nazmul Islam, Yogesh Singh, Jose A. Rodriguez-Rivera, Tatiana Guidi, Elisa M. Wheeler, Giovanna G. Simeoni, and Hanjo Ryll, “Magnetic Hamiltonian and phase diagram of the quantum spin liquid $\text{Ca}_{10}\text{Cr}_7\text{O}_{28}$,” *Phys. Rev. B* **95**, 174414 (2017).
 - [3] D. A. Garanin and Benjamin Canals, “Classical spin liquid: Exact solution for the infinite-component antiferromagnetic model on the kagomé lattice,” *Phys. Rev. B* **59**, 443–456 (1999).
 - [4] M. E. Zhitomirsky, “Octupolar ordering of classical kagome antiferromagnets in two and three dimensions,” *Phys. Rev. B* **78**, 094423 (2008).
 - [5] Mathieu Taillefumier, Julien Robert, Christopher L. Henley, Roderich Moessner, and Benjamin Canals, “Semiclassical spin dynamics of the antiferromagnetic Heisenberg model on the kagome lattice,” *Phys. Rev. B* **90**, 064419 (2014).
 - [6] J. Robert, B. Canals, V. Simonet, and R. Ballou, “Propagation and ghosts in the classical kagome antiferromagnet,” *Phys. Rev. Lett.* **101**, 117207 (2008).
 - [7] H. Yan, R. Pohle, and N. Shannon, in preparation.